Author/s:
Kim, S;Heath, DE;Kentish, SE

Title:
Improved carbon dioxide stripping by membrane contactors using hydrophobic electrospun poly(vinylidene fluoride-co-hexafluoro propylene) (PVDF-HFP) membranes

Date:
2022-01-15

Citation:
Kim, S., Heath, D. E. & Kentish, S. E. (2022). Improved carbon dioxide stripping by membrane contactors using hydrophobic electrospun poly(vinylidene fluoride-co-hexafluoro propylene) (PVDF-HFP) membranes. Chemical Engineering Journal, 428, https://doi.org/10.1016/j.cej.2021.131247.

Persistent Link:
https://hdl.handle.net/11343/281412

Improved carbon dioxide stripping by membrane contactors using hydrophobic electrospun poly(vinylidene fluoride-co-hexafluoro propylene) (PVDF-HFP) membranes

Seungju Kim [a], Daniel E. Heath [b], Sandra E. Kentish [*a]

[a] Department of Chemical Engineering, The University of Melbourne, Parkville, VIC 3010, Australia

[b] Department of Biomedical Engineering, The University of Melbourne, Parkville, VIC 3010, Australia

Abstract

Electrospun poly(vinylidene fluoride-co-hexafluoro propylene) (PVDF-HFP) nanofibre membranes are developed for CO_2 stripping within a membrane contactor. The porous and hydrophobic nature of the membranes is ideal for membrane CO_2 stripping applications, providing fast gas transport, high CO_2 recovery and mechanical strength. Three different morphologies of the PVDF-HFP membranes are assessed: nanofibre membranes (NFM), bead-on-string membranes (NFM-BS) and microparticles on nanofibre membranes (NFM-MP). We illustrate that both the bead-on-string and microparticles on nanofibre membranes are more hydrophobic compared to nanofibre constructs and a traditional asymmetric control membrane. The NFM-BS and NFM-MP membranes both exhibit significantly improved CO_2 stripping flux over short times, while the NFM-BS membranes provides significantly improved stripping flux over longer times (240 h) compared to all other treatments, including conventional asymmetric phase inversion membranes. The structures may also show promise for membrane distillation applications.

Keywords:

Membrane contactor, PVDF, electrospinning, membrane CO_2 stripping, CO_2 separation

1. Introduction

CO_2 removal from gas streams is an increasingly important separation process due to climate change. Solvent absorption processes have provided reliable performance for such separation processes for many decades, with the capability to remove well over 90% of the CO_2 [1]. In these processes, a packed column is used for CO_2 absorption from a gas into a solvent; and for CO_2 stripping, where pure CO_2 is released from the solvent under conditions of higher temperature or lower partial pressure, regenerating the solvent. Unlike such conventional packed column processes, a membrane contactor provides smaller equipment sizes with high packing density and easier solvent regeneration below the vaporisation temperature [2-5]. This leads to energy efficient CO_2 absorption and stripping. CO_2 separation from gases such as nitrogen in flue gas or methane in natural gas occurs due to the difference in gas solubility in the solvent, achieving excellent CO_2 selectivity [6-8]. The contactors are selective to CO_2 at low concentrations and partial pressures and the technology is thus widely adaptable to a range of applications in CO_2 separation from biogas, syngas, natural gas, or flue gas from power generation. Further, the heat transfer required for CO_2 stripping can be provided directly through a low pressure steam sweep, allowing for regeneration temperatures that are lower than in conventional desorbers [9, 10]. Moreover, the modular design of membrane contactors enables facile system scale-up, providing strong potential for larger scale operations evidenced by numerous pilot plant trials for CO_2 removal [11-13].

Hydrophobic nanofibre membranes prepared by electrospinning have been of research interest for numerous separation applications [14-16]. For instance, nanofibre membranes using hydrophobic polymers have a critical role in membrane distillation, particularly as a next generation membrane for seawater desalination [15]. While electrospun membranes have not been extensively studied for CO_2 stripping applications, the properties required for this application are similar to those for membrane distillation. Specifically, gas transport through

these membrane contactors is dominated by gas diffusion through the membrane pores. Wetting of these membrane pores by the solvent significantly decreases the transfer rate by reducing the diffusion rate. Therefore, preventing membrane wetting by the solvent is essential to improve the performance of both unit operations if they are to be preferred over the traditional, yet energy intensive processes.

When aqueous solvent systems are used, membranes made from hydrophobic polymers can be used to minimise wetting of the membrane. Hydrophobic polymers such as polypropylene (PP), polyvinylidene difluoride (PVDF), and polytetrafluoroethylene (PTFE) have been used widely for this purpose [17-20]. PVDF is one of the most investigated membrane materials because it is easily processed into various types of membranes such as electrospun nanofibres, flat sheets, and hollow fibres and exhibits excellent hydrophobicity.

Despite their promise, PVDF membranes have not achieved commercial success in CO_2 absorption applications because the intrinsic hydrophobicity of PVDF is not enough to completely prevent membrane wetting. For instance, Lin et al. reported PVDF nanofibre membranes as a composite with polydimethylsiloxane on alumina ceramic support for CO_2 absorption [21]. Despite having excellent absorption flux because of their high porosity, the nanofibre membranes were wetted by the amine solvent, resulting in continuous flux decline with time. As such, more hydrophobic base polymers or surface modifications that increase surface hydrophobicity are required. For instance, Lin et al. modified the nanofibers after fabrication with fluoroalkylsilanes to further increase the hydrophobicity [22-24]. While the grafting of fluorocarbon chains on the membrane surface is known to effectively improve the hydrophobicity, this technique is not ideal as it can lead to release of potentially toxic and environmentally harmful chemicals and requires a post-modification step that limits scalability and increases cost [24].

An alternative method for increasing the hydrophobicity of electrospun membranes is to structurally change the surface of the nanofibers. For instance, researchers have incorporated inorganic nanoparticles such as fluorinated TiO_2 or silica to increase surface roughness and hydrophobicity [25, 26]. However, this technique is limited by poor affinity between the polymer and the inorganic particles, often resulting in the particles detaching from the surface over time. The affinity between particles and polymers can be improved by coating the polymer with polymeric particles of the same composition. Polymer nanoparticles can be prepared by re-precipitation of a polymer from a solution using a non-solvent and stabiliser, but the resulting nanoparticles are not uniform in size [15]. Furthermore, the additional steps associated with particle production and adsorption reduce the scalability and increase the cost of the resulting membranes. A method of directly incorporating polymer beads into the structure during fabrication is desirable.

One method by which micro/nanoparticles might be incorporated into electrospun structures during fabrication is by producing the so called “bead-on-string” structure. Commonly, the goal of electrospinning is to avoid such a structure and rather to produce thin fibres with monodispered diameters. However, electrospinning conditions such as solution viscosity and concentration can be manipulated to instead produce nanofibres with large beads strung on a narrow nanofibre; or to produce discrete nanoparticles [27]. Such purposeful creation of beads on the electrospun fibres during deposition provides a facile and more scalable method of increasing the hydrophobicity of the membranes through an increase in the surface roughness [28]. Despite this potential advantage, bead-on-string structures often occur alongside a significant reduction in the mechanical strength of the nanofibres [29].

In this study, we test the hypothesis that electrospun membranes made from hydrophobic polymers with a bead-on-string morphology will exhibit superior performance as membrane gas-solvent contactors for CO_2 removal, a hypothesis that is supported by the data.

We fabricate the electrospun membranes from poly(vinylidene fluoride-co-hexafluoro propylene) (PVDF-HFP), which is inherently more hydrophobic than traditional PVDF due to the fluorine rich HFP moieties and has shown promise in previous studies of CO_2 stripping [30] and membrane distillation [31]. As the HFP component is fully fluorinated, the PVDF-HFP copolymer is also more resistant to degradation in alkali solution [32, 33], an imperative for CO_2 stripping applications. We fabricate the PVDF-HFP into novel electrospun membranes with bead-on-string structures to further improve the hydrophobicity compared to standard nanofibers by increasing the surface roughness of the fibres. The CO_2 stripping properties of the nanofibre membranes are then characterised with potassium glycinate aqueous solution as a CO_2 absorbent.

2. Experimental

2.1. Materials

Poly(vinylidene fluoride-co-hexafluoro propylene) (PVDF-HFP, average M_w 455,000), *N*,*N*-dimethylacetamide (DMAc, 99.8%), Acetone (99.5%), 2-propanol (99.5%) methyl orange and sulfuric acid (H_2SO_4, 95%) were purchased from Sigma-Aldrich (St Louis, MO) and used without further purification. Glycine (98.5%) and potassium hydroxide (85%) were purchased from Thermo Fisher Scientific (Waltham, MA). CO_2 (99.99%) and N_2 (99.99%) were supplied by Core gas (Thomastown, Australia).

2.2. Preparation of hydrophobic nanofibre membranes

Freestanding PVDF-HFP nanofibre membranes were prepared by electrospinning from PVDF-HFP solution. The polymer solution was prepared in a co-solvent of DMAc and acetone (7:3 w/w) at room temperature by vigorous stirring. Solutions of 8 wt% to 22 wt% were respectively prepared for uniform nanofibres, bead-on-string structures and microparticles.

After complete dissolution, the solutions were held at room temperature for 24 h for degassing. The 20 wt% polymer solution was placed into a syringe pump (Adelab Scientific, Thebarton, Australia) connected to a single spray needle tip within an electrospinning device consisting of a high voltage power supply (Spellman CZE1000R, Hauppauge, NY) and a grounded rotating steel drum collector with diameter of 5 cm and length of 15 cm. The tangential speed of the drum surface was fixed at 40 cm s^{-1} (150 rpm). The tip-to-collector distance was fixed at 10 cm and the tip was moved on a rail at a rate of 10 cm min^{-1} using a Linear Translation Stage from Thorlabs Inc. (Newton, NJ). The needle was charged at 12 kV and the solution injection rate was fixed at 1.5 ml h^{-1}. 4.0 ml of the polymer solution was electrospun to build a freestanding nanofibre coupon, named as a nanofibre membrane (NFM). For the bead-on-string nanofibre membrane (NFM-BS), an additional 0.2 ml of the 12 wt% to 18 wt% polymer solution was electrospun onto a freestanding NFM coupon at the same conditions as above. For the microparticles on nanofibre membrane (NFM-MP), 0.2 ml of the 8 wt% polymer solution was electrosprayed on a freestanding NFM coupon.

As a comparison, PVDF-HFP asymmetric membranes were prepared by non-solvent induced phase inversion from a solution containing PVDF-HFP in 20 wt% DMAc. The polymer solution was cast on a glass plate using a doctor blade and immediately immersed in ethanol for phase inversion for a day. The resulting asymmetric membranes were further rinsed in a water bath for 12 h and dried at room temperature.

2.3. Characterisation

The viscosity of the polymer solution was measured using a modular compact rheometer (MCR 702 TwinDrive, Anton Paar, Graz, Austria). The morphology of the electrospun membranes were investigated using a scanning electron microscope (SEM, FlexSEM, Hitachi, Tokyo, Japan). The membrane hydrophobicity was characterised using a

tensiometer (OCA 20, DataPhysics Instruments, Filderstadt, Germany). A sessile drop technique was used to measure the contact angle of the membrane surface. The breakthrough pressure (p_B) or so-called critical entry pressure of water is the pressure recorded when the first water droplet is observed on the permeate surface of the membrane. This breakthrough pressure was measured using a dead-end filtration cell (HP4750, Sterlitech, Kent, WA), but modified to visualise water droplets at the permeate surface. Increasing pressure was applied in 5 kPa intervals each 10 mins to detect the water droplets.

The maximum pore size (d_{max}) was calculated by the Young-Laplace equation from the breakthrough pressure of 20 wt% aqueous 2-propanol solution [34].

$$p_B = \frac{4\gamma cos\theta}{d_{max}}, \qquad d_{max} = \frac{4\gamma cos\theta}{p_B} \tag{1}$$

where d_{max} is the maximum pore diameter, γ is the surface tension of 2-propanol solution (34 x 10^{-3} N m^{-1}), and θ(°) is the contact angle of a 2-propanol solution with the membrane.

The average pore size ($d_{average}$) and the effective surface porosity (ε/L_p) of the membranes were determined from gas permeance measurement (j_i, mol m^{-2} Pa^{-1} s^{-1}) at elevated pressure ($\bar{P}$) using nitrogen accounting for both the Poiseuille flow and Knudsen flow mechanisms [35-37].

$$j_i = \frac{2r_p\varepsilon}{3RTL_P}\left(\frac{8RT}{\pi M}\right)^{0.5} + \frac{{r_p}^2\varepsilon}{8\mu_i RTL_P}\bar{P} \tag{2}$$

$$j_i = K_0 + P_0\bar{P} \tag{3}$$

Based on Equations 2 and 3:

$$r_p = \frac{16}{3}\left(\frac{P_0}{K_0}\right)\left(\frac{8RT}{\pi M}\right)^{0.5}\mu_i \tag{4}$$

$$d_{average} = 2r_p \tag{5}$$

$$\frac{\varepsilon}{L_P} = \frac{8\mu_i RTP_0}{{r_p}^2} \tag{6}$$

r_p (μm) is the average pore radius, ε/L_p (m^{-1}) is the effective surface porosity, R is the universal gas constant (J mol^{-1} K^{-1}), T is the absolute temperature (K), M is the molecular weight of nitrogen, and μ_i is the viscosity of nitrogen at 25 °C (1.78 x 10^{-5} Pa s).

The porosity of the membrane supports was determined by comparing the weight of dry and wet samples using kerosene of density of 0.8 g mL^{-1} by the following equation [16].

$$Porosity\ (\varepsilon) = \frac{W_w - W_d}{Ad\rho} \quad (7)$$

where W_w and W_d (g) are the weight of the wet and dry samples, A (m^2) is the surface area, d (μm) is the average thickness of the membrane supports and ρ is the kerosene density (g cm^{-3}).

2.4. CO_2 stripping Experiments

CO_2 stripping was investigated using a flat sheet membrane test unit, described in Fig. 1 [34, 38]. The stainless-steel membrane holder with an effective membrane area of 14.6 cm was manufactured in-house with holes for gas contact and a recessed gas channel for the gas flow. N_2 was fed into this gas channel in a range of 30 to 90 ml min^{-1} as a sweep gas to remove the permeating CO_2 to a vent.

The upper solvent chamber contained a magnetically driven stirrer to generate turbulence of the liquid layer, connected to an electronic stirrer motor (Heidolph Instruments, Model RZR 2020, Germany) operating at 100 rpm. The membrane holder was located in a convection oven and the temperature was controlled between 60 and 100 °C. The solvent was 30 wt% potassium glycinate (PG) solution prepared by adding equimolar amounts of potassium hydroxide and glycine to deionised water, giving a solution of initial pH 14. This solvent was pre-loaded with CO_2 by bubbling of pure CO_2 through the solution for 120 minutes, reducing the pH to 10. This pre-loaded solventwas fed into the solvent chamber using a peristaltic pump connected with silicone tubing, ID 4.8 mm (MasterFlex® L/S®, Cole-Parmer, Vernon Hills, IL).

The CO_2 stripping flux was calculated from the CO_2 concentration of both the inlet and outlet solvent streams by titration using a 0.4 M H_2SO_4 solution as the titrant and methyl orange as the indicator.

$$J_{CO2} = \frac{(C_{l.i} - C_{l.o}) \times Q_l}{A} = K \times C_{LM} \quad (8)$$

where J_{CO2} is the CO_2 stripping flux (mol m^{-2} s^{-1}), Q_l is the liquid flow rate (m^3 s^{-1}), $C_{l.i}$ is the CO_2 concentration (mol m^{-3}) at the solvent inlet, $C_{l.o}$ is the CO_2 concentration at the solvent outlet and A is the membrane effective area (m^2). C_{LM} (mol_{CO2} m^{-3}) is the log mean average of inlet and outlet concentrations of CO_2. K (m s^{-1}) represents the overall mass transfer coefficient [39], which is expressed as [38]:

$$\frac{1}{K} = \frac{m}{k_L E} + \frac{1}{k_m} + \frac{1}{k_G}, \qquad \frac{1}{K} = R_L + R_m + R_G \quad (9)$$

Where m is the partition coefficient, E is the enhancement factor, k_L, k_m and k_G are the mass transfer coefficients in the liquid, membrane and gas phases, and R_L, R_m and R_G are the mass transfer resistance of the liquid, membrane and gas phases.

The so-called Wilson plot method can be used to extract the membrane resistance (R_m) from experimental studies of the mass transfer of CO_2 at variable liquid phase flowrates [40, 41]. The liquid phase mass transfer resistance is a direct function of the Reynolds number and so at a controlled temperature can be defined as $1/R_L = Av^a$, where A and a are constant and v (m s^{-1}) is the solvent flowrate. The overall mass transfer resistance ($1/K$) is then defined as:

$$\frac{1}{K} = R_L + R_m + R_G = \frac{1}{Av^a} + R_m + R_G \quad (10)$$

A plot of $1/K$ versus v^{-a} will then be a straight line, with the y-intercept equal to $R_m + R_G$. In most cases, the gas phase resistance is negligible and hence this intercept directly reflects the membrane resistance.

The long-term CO_2 stripping performance was measured by continuous operation at 100 °C with a solvent flowrate of 100 ml min^{-1} and gas flowrate of 70 ml min^{-1}. The CO_2 pre-

loaded PG solution was injected into the membrane cell and the CO_2 concentration in the PG solution at the inlet and outlet channel of the membrane cell was measured by titration. Pure CO_2 gas was bubbled into the solvent tank every 3 hours to maintain the CO_2 concentration at a maximum.

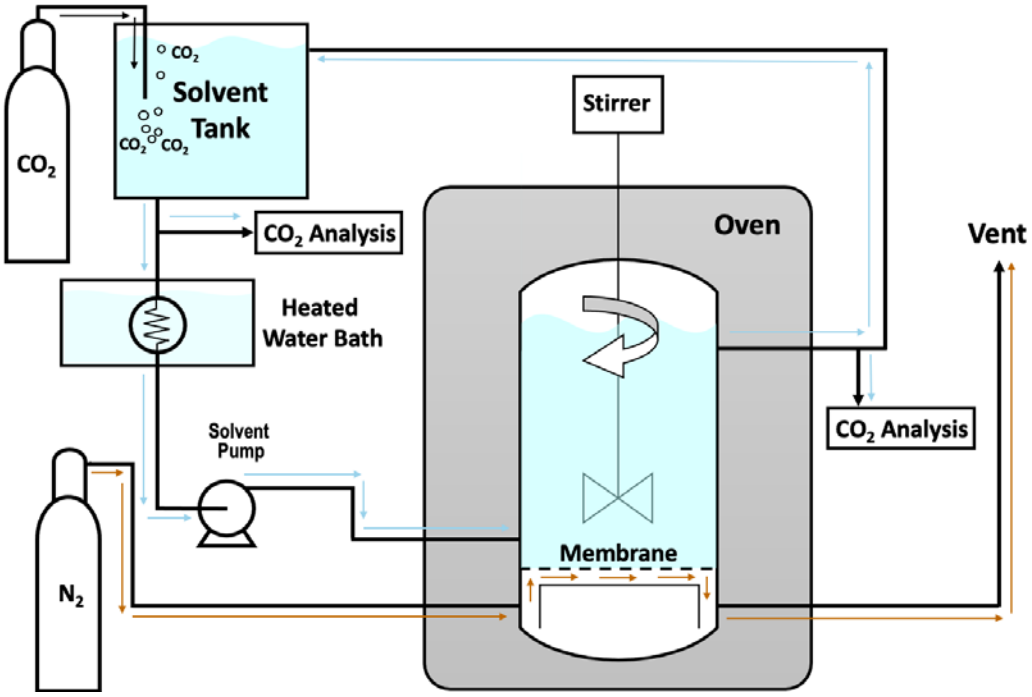

Fig. 1. Schematic diagram illustrating the piping layout for the flat sheet configuration for CO_2 stripping.

3. Results and discussion

Electrospinning and electrospraying are facile fabrication methods for fibres and particles, respectively. Fibres and bead of varying size and morphology can be generated by controlling electrospinning parameters such as electric field strength, solution conductivity, surface tension and viscosity, polymer concentration and molecular weight, collector size and shape, system temperature and humidity [14]. Commonly, electrospinning parameters are optimised to produce uniform ultrathin nanofibres with high porosity and relatively

monodispersed fibre diameter. However, insufficient stretching of the fibre jet during spinning eliminates the balance between the viscoelastic forces, surface tension and electrostatic repulsion, resulting in the formation of beads on the nanofibres [42, 43].

As illustrated schematically in Fig. 2, we fabricated membranes with three distinct morphologies. The first structure is a traditional nanofibre membrane (NFM). The second structure was a nanofibre membrane that had a layer of bead-on-string nanofibres deposited on the surface (NFM-BS). We chose to make a dual-layered structure for the NFM-BS because the bead-on-string structures can reduce the mechanical strength of the membrane [28, 29]. The NFM-BS structure results in membranes with similar strength to the NFM, yet increased surface roughness. The third structure was a nanofibre membrane that had microparticles deposited on the surface (NFM-MP). We hypothesised that the increased surface roughness generated by the bead-on-string structure or the presence of the nanoparticles would increase the apparent hydrophobicity of the resulting membranes, leading to less membrane wetting and superior CO_2 stripping.

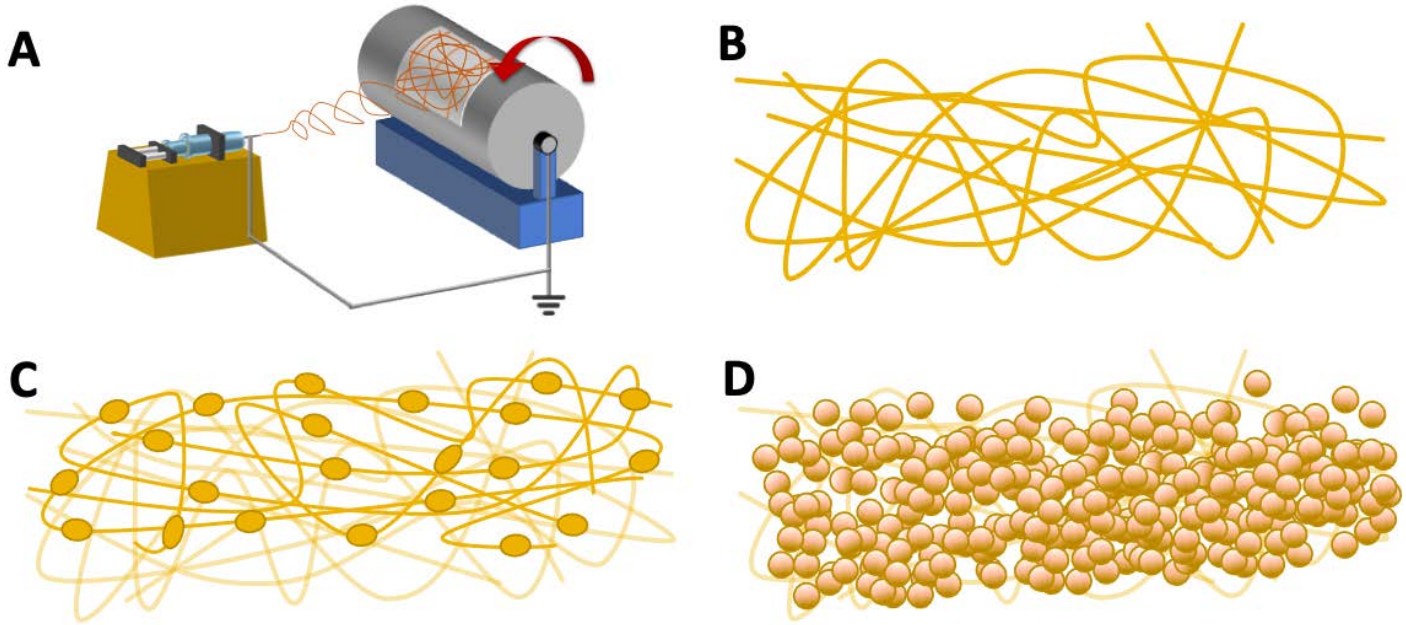

Fig. 2. Illustration of a nanofibre composite membrane, showing (a) the method to prepare electrospun nanofibres, (b) a uniform nanofibre membrane (NFM), (c) a bead-on-string structure on a nanofibre (NFM-BS), and (d) microparticles on a nanofibre (NFM-MP).

Table 1. The characteristics of the electrospun membranes as a function of polymer solution concentrations.

Polymer concentration (wt%)	Solution viscosity (cP)	Morphology	Size of particles or beads (μm)	Diameter of nanofibres (nm)	Density of beads (%)	Sample name
8	210 ± 20	Microparticle	1.5 ± 0.3	-	-	NFM-MP
10	250 ± 30	Microparticle	1.8 ± 0.5	-	-	-
12	760 ± 20	Bead-on-string	2.0 ± 0.3	200 ± 20	72	NFM-BS72
14	1090 ± 50	Bead-on-string	2.0 ± 0.3	200 ± 20	67	NFM-BS67
16	1420 ± 50	Bead-on-string	1.3 ± 0.3	250 ± 30	61	NFM-BS61
18	1960 ± 40	Bead-on-string	0.5 ± 0.1	300 ± 50	5	NFM-BS05
20	3370 ± 30	Nanofibre	-	300 ± 50	-	NFM
22	4830 ± 50	Nanofibre	-	600 ± 30	-	-

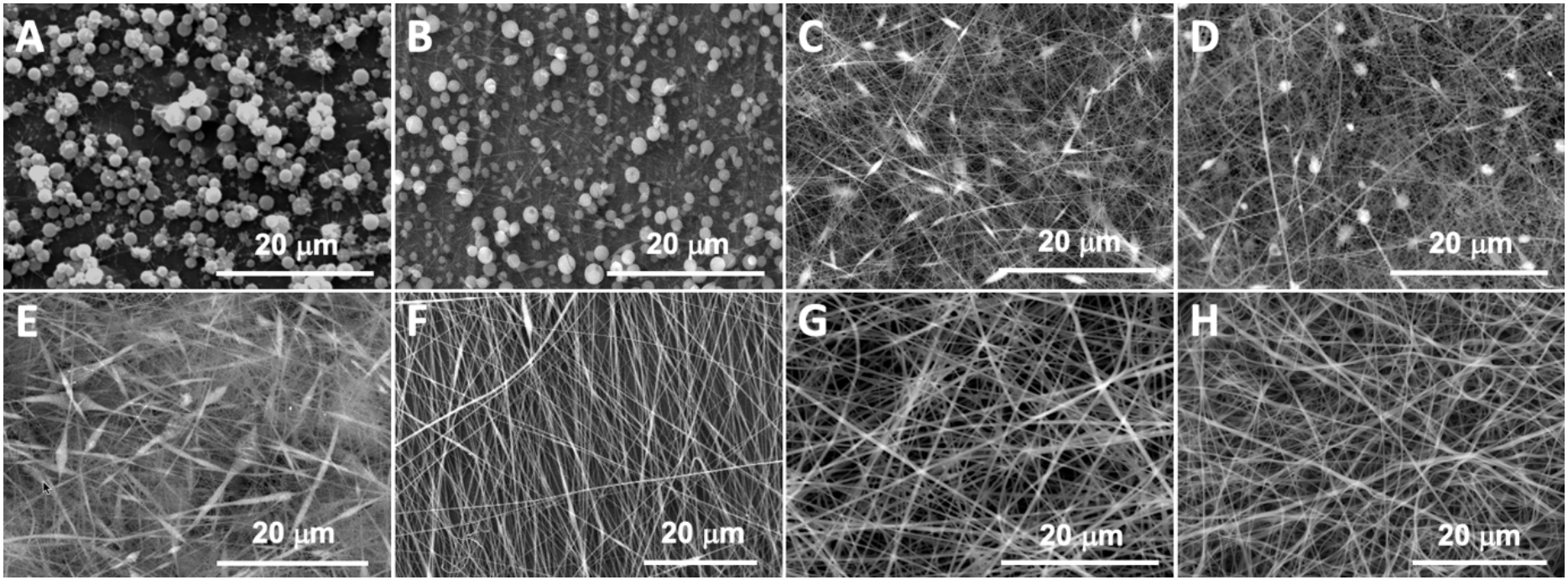

Fig. 3. Surface SEM images of electrospun membranes prepared from (a) 8 wt%, (b) 10 wt%, (c) 12 wt%, (d) 14 wt%, (e) 16 wt%, (f) 18 wt%, (g) 20 wt%, and (h) 22 wt% solution.

The tip-to-collector distance, applied voltage and polymer concentration were first optimised to produce ultrafine nanofibres. The resulting freestanding nanofibre membranes were prepared from 20 wt% PVDF-HFP, had a nanofibre diameter around 300 nm and a membrane thickness of 100 μm. The use of PVDF-HFP for both the substrate and the coating layer improved the affinity and adhesion between the two layers.

The solution concentration was then varied between 8 and 22 wt% to alter the solution viscosity, which ranged between 210 to 4830 cP. In turn, this affected the nanofibre morphology. The solutions of 8 wt% and 10 wt% produced microparticles. These microparticles were uniform in diameter as they were prepared by so-called electrospraying; the solution did not form a Taylor cone at the needle tip, but rather polymer droplets were sprayed onto the collector. The nanofibres underneath the layers are not visible at 8 wt%, indicating that the microparticles form a continuous layer. When concentration increases to 10 wt%, strings connecting the microparticles became visible. The solutions of 12 wt% to 18 wt% result in the bead-on-string morphology, with the density of beads decreasing as solution concentrations are increased. Uniform nanofibres appear at 20 to 22 wt% polymer.

The layers of bead-on-string or microparticles were deposited as fibres of 200 nm on the freestanding nanofibre mat, with bead diameters of 0.5 to 2 μm (Fig. 3c-f) and microparticle diameters of 1.5 to 1.8 μm (Fig. 3a,b). The fibre (string) diameter is generally thinner than for uniform nanofibres because this unique morphology is formed by unstable solvent evaporation with polymer phase inversion [42].

The asymmetric PVDF-HFP membranes presented a contact angle of 105° while the electrospun membranes all presented greater contact angles indicative of greater hydrophobicity (Fig. 4a). The surface morphology clearly affected the hydrophobicity of the membrane surface due to the differences in surface roughness despite using the same material, with the contact angle greater for the bead-on-string and microparticle loaded membranes than

for the uniform nanofibre material. This observation is consistent with a previous report by Singh et al. that phosphazene-based polymer nanofibres with bead-on-string structures showed a higher water contact angle than uniform nanofibres [28]. Unlike asymmetric membranes with a flat surface, the space between the nanofibres forms a gas pocket when exposed to water which increases the contact angle (Fig. 4b) by increasing the solid surface energy and solid-liquid surface tension as indicated in Young's equation [44]. According to the Cassie model, an air pocket is formed on a rough surface and water droplets remain unpinned to the surface [45]. The microparticles or beads further increase the size of the gas pocket, leading to enhanced hydrophobicity.

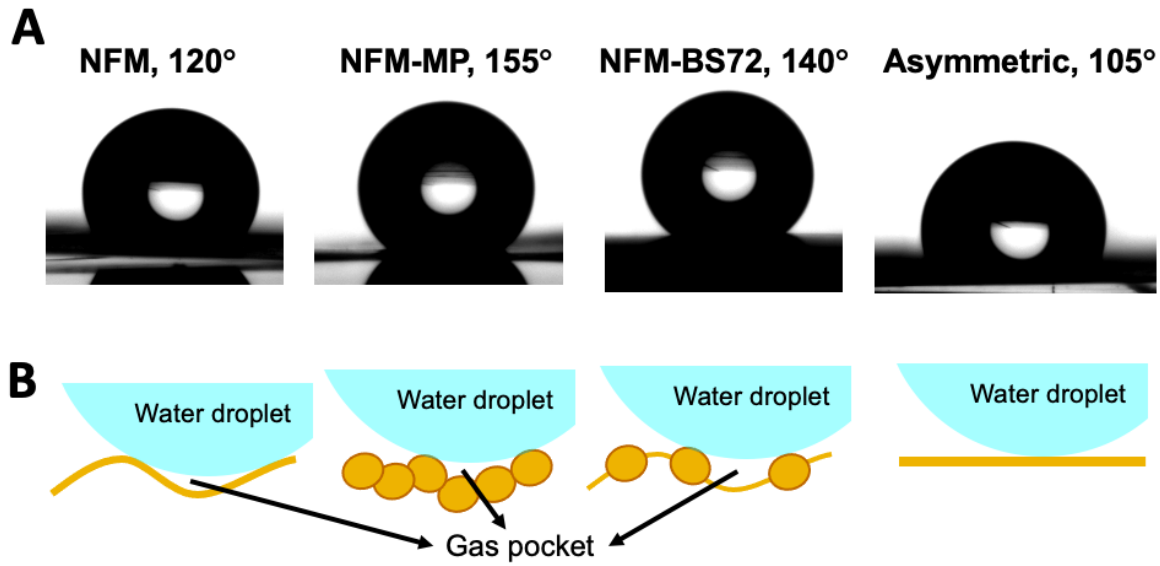

Fig. 4. (a) Water contact angle of PVDF-HFP membranes and (b) schematic representation of the surface structures with water droplet.

The use of a thin layer of bead-on-string or microparticles did not affect the bulk properties of the membranes but the surface properties were changed after coating, as summarised in Table 2. The overall porosities of the NFM, NFM-BS72 and NFM-MP were 83, 82 and 83 %, respectively, which are much higher than that of the asymmetric membrane, at

68 %. This high porosity of electrospun nanofibres is generally attributed to the overlapping fibre structures during electrospinning [46]. Since the overall porosity is mainly determined by the nanofibrous substrate, all three membranes possessed similarly high porosity. The asymmetric membranes exhibited the greatest breakthrough pressure of 350 kPa, which relates to their low porosity and is similar to other PVDF asymmetric membranes used in membrane gas-liquid contactors [44]. NFM, NFM-BS72 and NFM-MP exhibited values of 120, 140 and 155 kPa, respectively. Other PVDF-based nanofibre membranes developed for membrane distillation show similar breakthrough pressures in the range of 25-200 kPa [47]. The maximum pore sizes (d_{max}) of the nanofibre membranes were higher than that of the asymmetric membranes, which is again characteristic of electrospun structures. These large pores are advantageous for CO_2 transport, but may not be small enough to prevent solvent penetration. The composite NFM-BS72 and NFM-MP membranes both have smaller pores than NFM however, due to the additional thin layer of beads or microparticles which reduces the space between the nanofibres. This trend is replicated with the average pore sizes ($d_{average}$) determined by gas permeance measurement, as shown in Table 2. The difference between d_{max} and $d_{average}$ is only between 0.01 to 0.06 μm, meaning that the membranes have narrow pore size distributions. The effective surface porosity (ε/L_p) indicates the proportion of pores that are connected through both sides of the membrane, so that the molecular transport can occur. This parameter was greater for the asymmetric membrane than the nanofibre membranes but the smaller pore sizes in this structure may also affect the mass transport properties.

Table 2. The characteristics of the prepared membranes.

	NFM	NFM-BS72	NFM-MP	Asymmetric
Overall porosity (%)	83 ± 3	82 ± 3	83 ± 2	68 ± 2
Water contact angle (°)	120 ± 2	140 ± 4	155 ± 3	105 ± 2
Water breakthrough pressure (critical entry pressure) (kPa)	120 ± 2	130 ± 2	135 ± 2	350 ± 3
Contact angle of IPA 20 wt% solution (°)	82 ± 1	83 ± 2	83 ± 1	78 ± 1
Breakthrough pressure of IPA solution (kPa)	39 ± 1	40 ± 1	43 ± 2	145 ± 3
d_{max} (μm) by breakthrough pressure of IPA solution	0.49	0.41	0.38	0.20
$d_{average}$ by N_2 permeance (μm)	0.43	0.40	0.37	0.17
Effective surface porosity (m^{-1})	150	155	159	199

The most widely used solvent for commercial-scale CO_2 capture is monoethanolamine (MEA). However, this solvent readily degrades the materials and glues used in membrane contactors; is volatile leading to solvent loss; and requires a high regeneration energy [44]. In this work, an aqueous PG solution was selected as an alternative solvent, as it is non-volatile, non-toxic and has much greater resistance to oxidative degradation [39, 48, 49]. The use of a non-volatile solvent is critical to the use of a membrane for CO_2 stripping at commercial scale, as it ensures that the low pressure steam sweep or vacuum used on the permeate side does not become contaminated with solvent due to evaporation. PG is an amino acid with comparable CO_2 solubility to MEA (0.4 to 0.7 $mol_{CO2}/mol_{solvent}$ for a 3.0 M PG solution at temperature between 20 to 50 °C [48]) and comparable absorption kinetics [50]. Such amino acids have been commercialised for CO_2 separation in the BASF Alkazid and Siemens PostCap processes [51].

Our focus was on the CO_2 stripping performance. During the stripping operation, the CO_2 flux is expected to increase with the operating temperature, as this increases the equilibrium CO_2 partial pressure of the solvent and thus the driving force for mass transfer. This behaviour is indeed observed for all membrane samples. The CO_2 stripping flux of the

NFM-BS membranes was first investigated to characterise the influence of the density of beads (Fig 5). While many of these results are identical within experimental error, the flux generally increased as the density of beads on the nanofibre increased, while the NFM-BS05 membrane provided a similar flux to the uniform NFM. Further, all nanofibre membranes exhibited a higher CO_2 flux than the asymmetric membranes, as the nanofibres with high porosity and large pore size led to fast molecular transport (Fig. 6). At 60 °C the difference in CO_2 flux was only minor, but at 100 °C, the NFM-MP and NFM-BS72 showed almost 200 % higher CO_2 flux than the asymmetric sample.

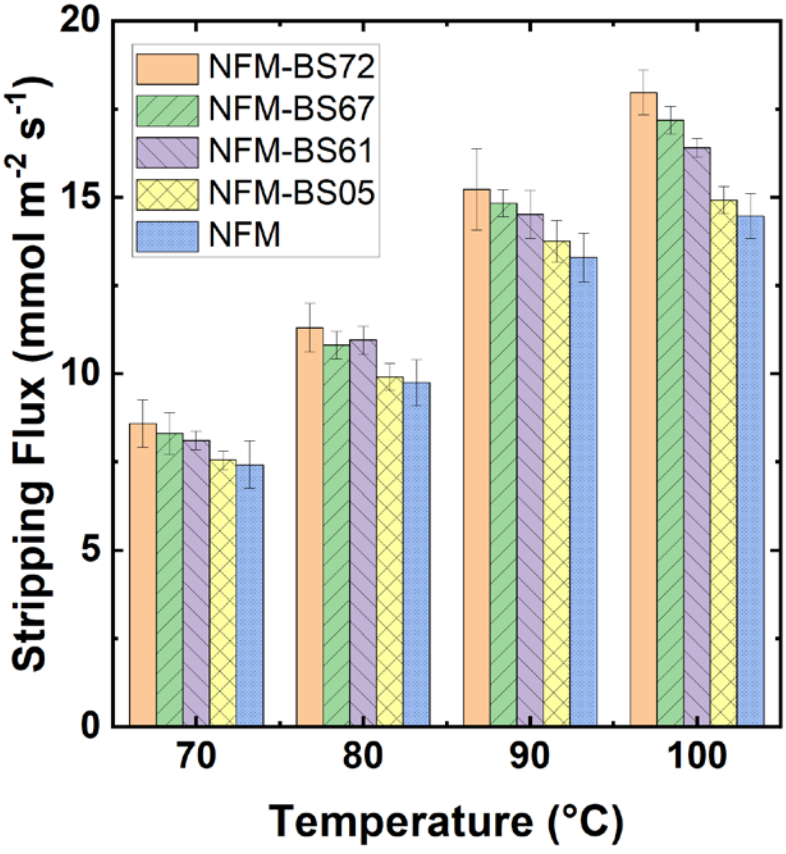

Fig. 5. CO_2 stripping flux of PVDF-HFP nanofibre membranes with different bead density. Solvent and gas flowrates were fixed at 100 and 70 ml min^{-1}, respectively.

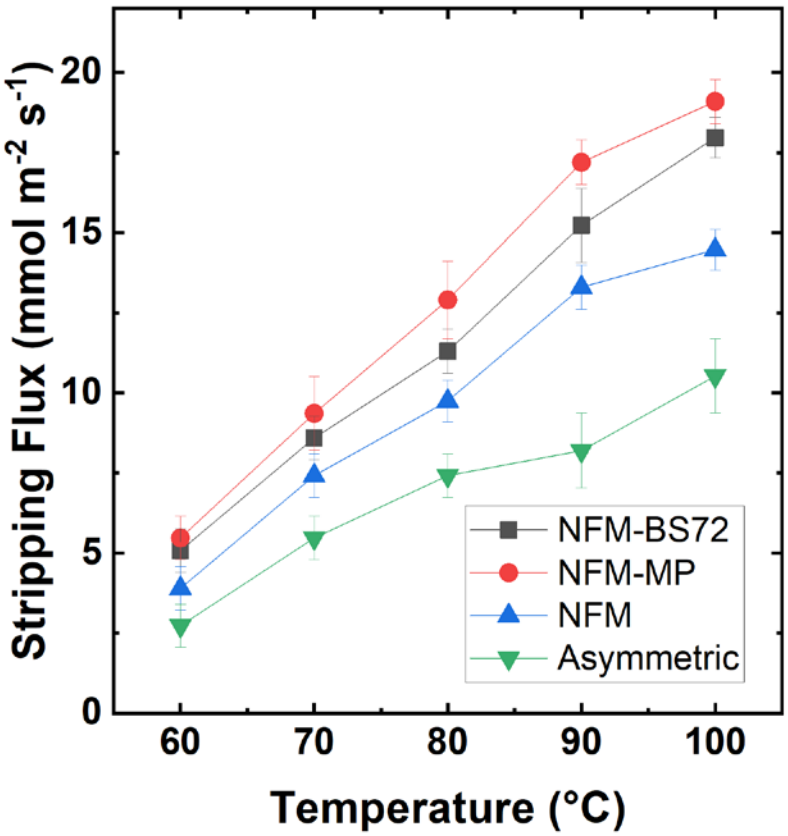

Fig. 6. CO_2 stripping flux of PVDF-HFP membranes as a function of operating temperature. Solvent and gas flowrates were fixed at 100 and 70 ml min^{-1}, respectively.

The CO_2 stripping flux is related not only to the membrane pore size and porosity, but also to the membrane hydrophobicity, as membrane wetting can fill these pores with solvent, hindering gas transport [44]. The improved surface hydrophobicity from the microparticles and bead-on-string effectively reduced this membrane wetting resulting in increased flux.

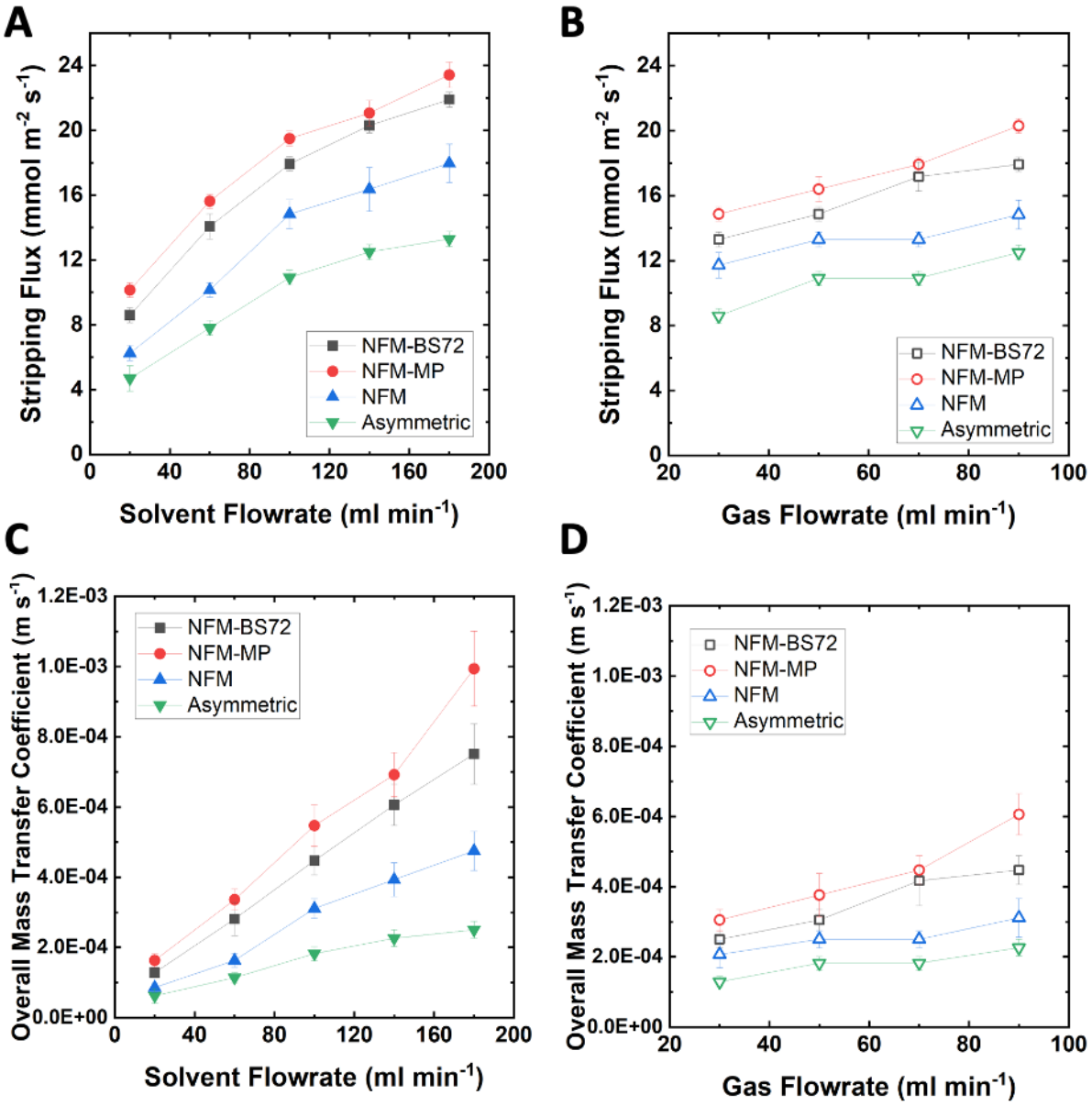

Fig. 7. CO_2 stripping flux and the overall mass transfer coefficient of PVDF-HFP membranes at 100 °C as a function of (a, c) solvent (the gas flowrate is at 70 ml min^{-1}) and (b, d) gas flowrates (the solvent flowrate is at 100 ml min^{-1}).

The mass transfer of CO_2 during a stripping operation is usually limited by the resistance of the membrane itself as described above. However, if this resistance is low, the CO_2 flux can also be influenced by the gas and liquid phase boundary layers. Low flowrates of gas or solvent can reduce the Reynolds numbers within these boundary layers, causing the mass

transfer resistances in these phases to increase. Indeed, Fig. 7 shows that the CO_2 flux and the overall mass transfer coefficient increased with both solvent and gas flowrate. The effect of solvent flowrate was more dramatic than that of gas flowrate, due to the greater viscosity of this phase. Since the overall mass transfer coefficient is the sum of the mass transfer coefficients at gas, liquid and membrane phases (Equation 9), the more dramatic increase by the solvent flowrate means that the CO_2 transfer is influenced mainly by the liquid phase mass transfer.

While N_2 is applied as a sweep gas in this study, saturated steam would be used in the industrial membrane CO_2 stripping process to simultaneously reduce the CO_2 partial pressure and draw CO_2 from the solvent, while providing a direct heating source [11]. The water vapour and stripped CO_2 are then easily separated using a condenser. However, when a high sweep flowrate is used, a large volume of steam must be condensed to separate CO_2, leading to a high energy consumption. Regardless of the gas or solvent flowrate used, the nanofibre membranes exhibited a higher CO_2 flux than the asymmetric membranes. The nanofibre membranes also showed stable performance without operational failure, indicating that the membranes provided sufficient mechanical strength for membrane CO_2 stripping applications.

The Wilson-plot method was employed to obtain the membrane mass transfer resistance as described in Fig. 8. The best fit of a straight line to the relationship between $1/K$ and v^{-a} (Equation 10) was found with a value of 0.8 for the parameter a with R^2 between 0.9984 to 0.99987. This value is consistent with correlations for transfer coefficients with the Reynolds Number generally found in the literature for turbulent flow [52]. The y-intercept provides a value of the combined membrane mass transfer resistance and gas phase resistance. However, as the overall mass transfer coefficient changes little with gas flowrate (Fig. 7d), it can be concluded that this intercept predominantly reflects the membrane value. The nanofibre membranes clearly have much lower resistance than the asymmetric membranes. The NFM

has slightly higher resistance than the NFM-BS72 and NFM-MP because of the reduced hydrophobicity on the membrane surface. The mass transfer resistance obtained at 100 °C with the gas and solvent flowrate of 70 and 100 ml min^{-1} in Fig. 8b confirms that that the vast majority of the overall mass transfer resistance of the nanofibre membranes comes from the liquid phase, while around 25% comes from the membrane for the asymmetric case.

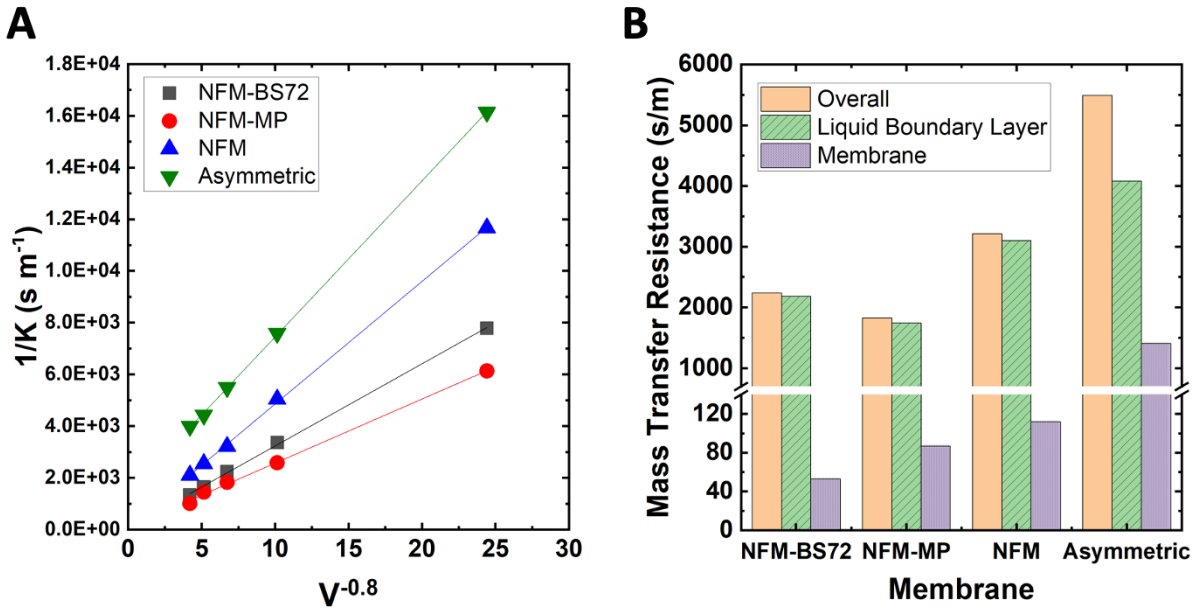

Fig. 8. (a) Wilson plot of PVDF-HFP membranes undergoing CO_2 membrane stripping at 100 °C with a gas flowrate of 70 ml min^{-1}, (b) components of the mass transfer resistance at a solvent flowrate of 100 ml min^{-1}.

Fresh membranes generally demonstrate a high flux that decreases with time due to partial or complete wetting. This pore wetting is difficult to reverse due to the capillary forces exerted once wetted [24, 44]. Most membranes even with sufficient hydrophobicity experience an initial flux decline by partial wetting. Fig. 9 describes the long-term CO_2 stripping performance of the nanofibre and asymmetric membranes. A flux decline of all four membranes was observed, but this generally stabilised after 240 h (10 days) of continuous

operation. The decline was greatest for the asymmetric membrane, which fell to only 13 % of the initial flux. This flux decline is generally observed in most PVDF asymmetric membranes, caused by partial wetting [24, 44]. However, the improved hydrophobicity of the nanofibrous morphology restricted membrane wetting and the flux decline. The NFM-MP membrane exhibited the highest initial CO_2 flux among the four samples, but its flux dramatically decreased with time. This is probably because the microparticles were only physically attached to the substrate and were readily removed by the solvent flow. After 60 h, the CO_2 flux of this membrane was similar to that of the NFM. On the other hand, the bead-on-string layer was firmly entwined with the nanofibre substrate so that the composite structure was not delaminated by solvent flow. The SEM images shown in Fig. 10 compare the surface morphology before (Fig. 10a) and after (Fig. 10b) the long-term CO_2 stripping measurement, confirming the loss of the coating layer of microparticles. On the other hand, the surface morphology of the NFM-BS72 membranes remained unchanged (Fig. 10d). This is also evidenced by the water contact angles after long-term measurement and then drying, described in Fig. 11. The membranes were rinsed with deionised water then exposed to ambient air for over a week before measurement. The contact angles of the NFM and NFM-BS72 membrane surfaces were unchanged, but that of NFM-MP reduced from 155° to 132°, reflecting the loss of the microparticles. The pores of the asymmetric membranes remain wetted even after the drying process, due to strong capillary forces [19], so that the surface hydrophobicity is permanently reduced. However, the nanofibre membranes showed possible restoration of surface hydrophobicity by pore drying, providing promise for long-term CO_2 separation applications.

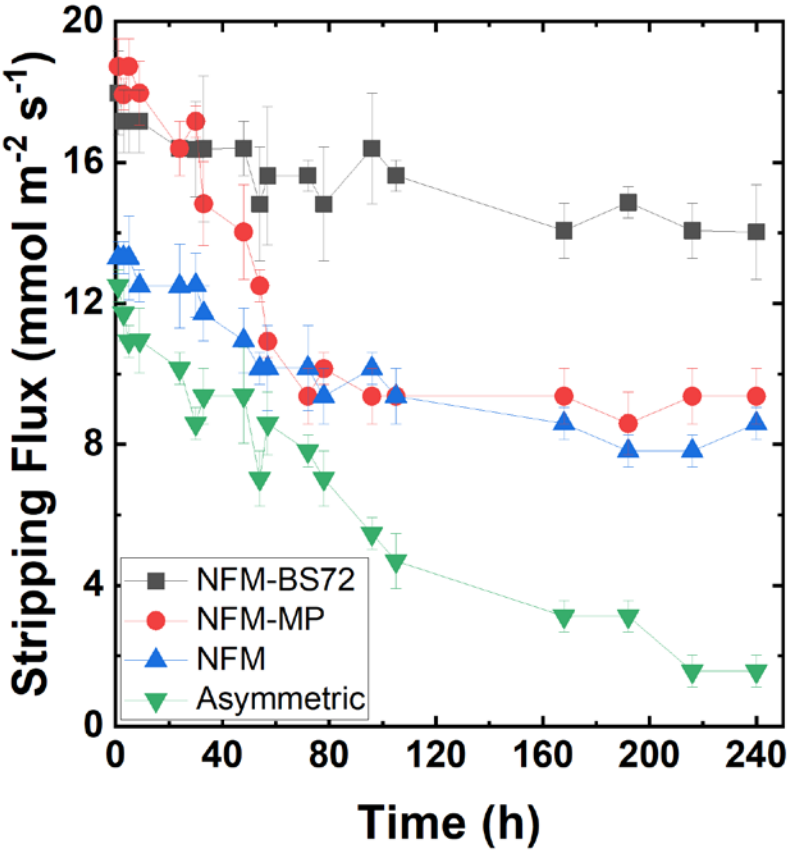

Fig. 9. Long-term CO_2 stripping performance of PVDF-HFP membranes, measured at 100 °C with a solvent flowrate of 100 ml min^{-1} and gas flowrate of 70 ml min^{-1}.

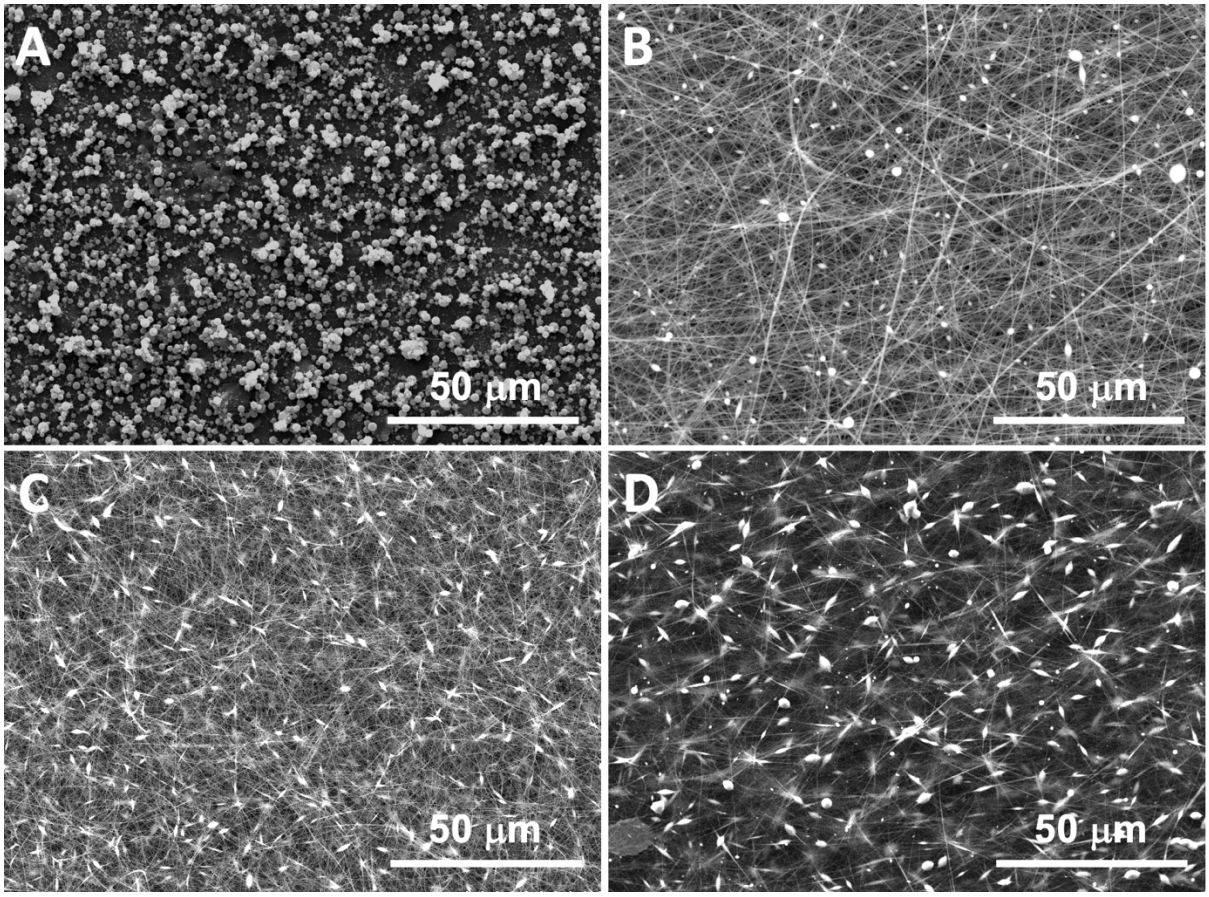

Fig. 10. Surface SEM images of NFM-MP (a) before and (b) after long-term operation and NFM-BS72 (c) before and (d) after long-term operation.

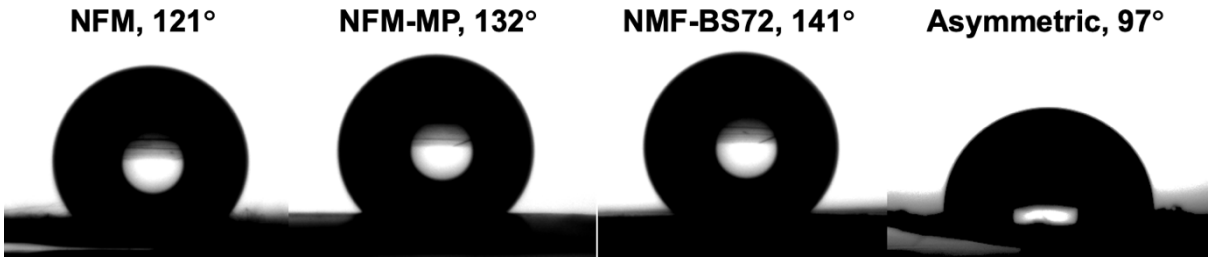

Fig. 11. Water contact angle of PVDF-HFP membranes after long-term operation and subsequent drying.

4. Conclusion

In summary, PVDF-HFP nanofibre composite membranes with both bead-on-string and microparticle surface layers were fabricated and showed enhanced CO_2 stripping performance in a membrane contactor arrangement. The morphology of the top layer was controlled by varying electrospinning parameters, chiefly solution viscosity, to obtain bead-on-string structures of variable bead density or microparticle structures which greatly improved the surface hydrophobicity. The nanofibrous composite membranes were more porous than conventional asymmetric membranes, resulting in a high CO_2 stripping flux and overall mass transfer coefficient, at temperatures up to 100 °C. Both the bead-on-string and microparticle composite membranes also outperformed a uniform electrospun nanofibre membrane due to the enhanced hydrophobicity, with a contact angle greater than 140° reducing membrane wetting. In particular, the mass transfer resistance of the membrane phase was greatly reduced for the nanofibre composite membranes as compared with asymmetric membranes, characterised by the Wilson plot method. In long term experiments, the microparticles were easily removed into the solvent flow, resulting in a CO_2 flux decline with time, evidenced by SEM images and a decrease in contact angle. However, the bead-on-string surface was stable for up to ten days, with no change in morphology. Importantly, this fabrication method is highly reproducible and can be further developed for large-scale production. This strategy is also promising for other membrane applications which require hydrophobic membranes such as membrane distillation.

Acknowledgement

This research was supported under the Australian Research Council Discovery Projects Scheme (Project number DP190102253). The authors acknowledge the staff of the Materials Characterisation and Fabrication Platform (MCFP) at the University of Melbourne and the

Victorian Node of the Australian National Fabrication Facility (ANFF) for their technical assistance.

References

[1] A.L. Kohl, R.B. Nielsen, Gas Purification (5th Edition), Elsevier.

[2] L. Ansaloni, A. Hartono, M. Awais, H.K. Knuutila, L. Deng, CO2 capture using highly viscous amine blends in non-porous membrane contactors, Chem. Eng. J. 359 (2019) 1581-1591.

[3] P.J. Gusnawan, S. Zha, L. Zou, G. Zhang, J. Yu, Soybean and moringa based green biosolvents for low-concentration CO2 capture via a hollow fiber membrane contactor, Chem. Eng. J. 335 (2018) 631-637.

[4] M. Rahbari-Sisakht, D. Rana, T. Matsuura, D. Emadzadeh, M. Padaki, A.F. Ismail, Study on CO2 stripping from water through novel surface modified PVDF hollow fiber membrane contactor, Chem. Eng. J. 246 (2014) 306-310.

[5] M. Li, Z. Zhu, M. Zhou, X. Jie, L. Wang, G. Kang, Y. Cao, Removal of CO2 from biogas by membrane contactor using PTFE hollow fibers with smaller diameter, J. Membr. Sci. 627 (2021) 119232.

[6] S.E. Kentish, 110th anniversary: process developments in carbon dioxide capture using membrane technology, Ind. Eng. Chem. Res. 58(28) (2019) 12868-12875.

[7] D. Hospital-Benito, J. Lemus, C. Moya, R. Santiago, V.R. Ferro, J. Palomar, Techno-economic feasibility of ionic liquids-based CO2 chemical capture processes, Chem. Eng. J. 407 (2021) 127196.

[8] Z. Pang, S. Jiang, C. Zhu, Y. Ma, T. Fu, Mass transfer of chemical absorption of CO2 in a serpentine minichannel, Chem. Eng. J. 414 (2021) 128791.

[9] Z. Wang, M. Fang, Q. Ma, Z. Zhao, T. Wang, Z. Luo, Membrane stripping technology for CO2 desorption from CO2-rich absorbents with low energy consumption, Energy Procedia 63 (2014) 765-772.

[10] P.J. Gusnawan, L. Zou, G. Zhang, J. Yu, Performance and stability of a bio-inspired soybean-based solvent for CO2 capture from flue gas, Chem. Eng. J. 385 (2020) 123908.

[11] C.A. Scholes, S.E. Kentish, A. Qader, Membrane gas-solvent contactor pilot plant trials for post-combustion CO2 capture, Sep. Purif. Technol. 237 (2020) 116470.

[12] C.A. Scholes, A. Qader, G.W. Stevens, S.E. Kentish, Membrane gas-solvent contactor pilot plant trials of CO2 absorption from flue gas, Sep. Sci. Technol. 49(16) (2014) 2449-2458.

[13] S. Li, T. Pyrzynski, T. Tamale, N. Klinghoffer, H. Meyer, J. Marion, Y. Ding, U. Shanbhag, E. Sanders, Pilot Test of a Nanoporous , Super hydrophobic Membrane Contactor Process for Post combustion CO2 Capture DOE NETL Project Review Meeting, Pittsburgh, PA, 2019.

[14] S. Kim, D.E. Heath, S.E. Kentish, Composite Membranes with Nanofibrous Cross-Hatched Supports for Reverse Osmosis Desalination, ACS Appl. Mater. Interfaces 12(40) (2020) 44720-44730.

[15] J.H. Kim, S.H. Park, M.J. Lee, S.M. Lee, W.H. Lee, K.H. Lee, N.R. Kang, H.J. Jo, J.F. Kim, E. Drioli, Thermally rearranged polymer membranes for desalination, Energy Environ. Sci. 9(3) (2016) 878-884.

[16] T.-D. Lu, B.-Z. Chen, J. Wang, T.-Z. Jia, X.-L. Cao, Y. Wang, W. Xing, C.H. Lau, S.-P. Sun, Electrospun nanofiber substrates that enhance polar solvent separation from organic compounds in thin-film composites, J. Mater. Chem. A 6(31) (2018) 15047-15056.

[17] D. deMontigny, P. Tontiwachwuthikul, A. Chakma, Using polypropylene and polytetrafluoroethylene membranes in a membrane contactor for CO2 absorption, J. Membr. Sci. 277(1) (2006) 99-107.

[18] C.A. Scholes, M. Simioni, A. Qader, G.W. Stevens, S.E. Kentish, Membrane gas–solvent contactor trials of CO2 absorption from syngas, Chem. Eng. J. 195-196 (2012) 188-197.

[19] C.A. Scholes, S.E. Kentish, G.W. Stevens, D. deMontigny, Comparison of thin film composite and microporous membrane contactors for CO2 absorption into monoethanolamine, Int. J. Greenh. Gas Control. 42 (2015) 66-74.

[20] C.-L. Huang, P.-Y. Wang, Y.-Y. Li, Fabrication of electrospun CO2 adsorption membrane for zinc-air battery application, Chem. Eng. J. 395 (2020) 125031.

[21] Y.-F. Lin, Q. Ye, S.-H. Hsu, T.-W. Chung, Reusable fluorocarbon-modified electrospun PDMS/PVDF nanofibrous membranes with excellent CO2 absorption performance, Chem. Eng. J. 284 (2016) 888-895.

[22] Y. Lin, Y. Xu, C.H. Loh, R. Wang, Development of robust fluorinated TiO2/PVDF composite hollow fiber membrane for CO2 capture in gas-liquid membrane contactor, Appl. Surf. Sci. 436 (2018) 670-681.

[23] Y. Xu, Y. Lin, M. Lee, C. Malde, R. Wang, Development of low mass-transfer-resistance fluorinated TiO2-SiO2/PVDF composite hollow fiber membrane used for biogas upgrading in gas-liquid membrane contactor, J. Membr. Sci. 552 (2018) 253-264.

[24] H. Pang, Z. Chen, H. Gong, M. Du, Fabrication of a super hydrophobic polyvinylidene fluoride–hexadecyltrimethoxysilane hybrid membrane for carbon dioxide absorption in a membrane contactor, J. Membr. Sci. 595 (2020) 117536.

[25] A. Razmjou, E. Arifin, G. Dong, J. Mansouri, V. Chen, Superhydrophobic modification of TiO2 nanocomposite PVDF membranes for applications in membrane distillation, J. Membr. Sci. 415-416 (2012) 850-863.

[26] Y. Liao, R. Wang, A.G. Fane, Fabrication of Bioinspired Composite Nanofiber Membranes with Robust Superhydrophobicity for Direct Contact Membrane Distillation, Environ. Sci. Technol. 48(11) (2014) 6335-6341.

[27] H. Fong, I. Chun, D.H. Reneker, Beaded nanofibers formed during electrospinning, Polymer 40(16) (1999) 4585-4592.

[28] A. Singh, L. Steely, H.R. Allcock, Poly [bis (2, 2, 2-trifluoroethoxy) phosphazene] superhydrophobic nanofibers, Langmuir 21(25) (2005) 11604-11607.

[29] Z.-M. Huang, Y.Z. Zhang, S. Ramakrishna, C.T. Lim, Electrospinning and mechanical characterization of gelatin nanofibers, Polymer 45(15) (2004) 5361-5368.

[30] S. Hosseini, A. Mansourizadeh, Preparation of porous hydrophobic poly (vinylidene fluoride-co-hexafluoropropylene) hollow fiber membrane contactors for CO2 stripping, J. Taiwan Inst. Chem. Eng. 76 (2017) 156-166.

[31] B.S. Lalia, E. Guillen-Burrieza, H.A. Arafat, R. Hashaikeh, Fabrication and characterization of polyvinylidenefluoride-co-hexafluoropropylene (PVDF-HFP) electrospun membranes for direct contact membrane distillation, J. Membr. Sci. 428 (2013) 104-115.

[32] V.F. Cardoso, D.M. Correia, C. Ribeiro, M.M. Fernandes, S. Lanceros-Méndez, Fluorinated polymers as smart materials for advanced biomedical applications, Polymers 10(2) (2018) 161.

[33] X. Wang, C. Xiao, H. Liu, Q. Huang, H. Fu, Fabrication and properties of PVDF and PVDF-HFP microfiltration membranes, J. Appl. Polym. Sci. 135(40) (2018) 46711.

[34] J.A. Franco, S.E. Kentish, J.M. Perera, G.W. Stevens, Poly (tetrafluoroethylene) sputtered polypropylene membranes for carbon dioxide separation in membrane gas absorption, Ind. Eng. Chem. Res. 50(7) (2011) 4011-4020.

[35] M. Rahbari-Sisakht, A. Ismail, T. Matsuura, Effect of bore fluid composition on structure and performance of asymmetric polysulfone hollow fiber membrane contactor for CO2 absorption, Sep. Purif. Technol. 88 (2012) 99-106.

[36] K. Li, Ceramic membranes for separation and reaction, John Wiley & Sons2007.

[37] G. Bakeri, A. Ismail, D. Rana, T. Matsuura, Development of high performance surface modified polyetherimide hollow fiber membrane for gas–liquid contacting processes, Chem. Eng. J. 198 (2012) 327-337.

[38] M. Simioni, S.E. Kentish, G.W. Stevens, Membrane stripping: Desorption of carbon dioxide from alkali solvents, J. Membr. Sci. 378(1) (2011) 18-27.

[39] E. Hosseini, E. Soroodan Miandoab, G.W. Stevens, C.A. Scholes, Absorption of CO2 from flue gas under oscillating gas flow conditions in gas-solvent hollow fibre membrane contactors, Sep. Purif. Technol. 249 (2020) 117151.

[40] E.E. Wilson, A basis for rational design of heat transfer apparatus, The J. Am. Soc. Mech. Engrs. 37 (1915) 546-551.

[41] E. Ataeivarjovi, Z. Tang, J. Chen, Study on CO2 Desorption Behavior of a PDMS–SiO2 Hybrid Membrane Applied in a Novel CO2 Capture Process, ACS Appl. Mater. Interfaces 10(34) (2018) 28992-29002.

[42] Z. Wang, C. Zhao, Z. Pan, Porous bead-on-string poly (lactic acid) fibrous membranes for air filtration, J. Colloid Interface Sci. 441 (2015) 121-129.

[43] M.M. Munir, A.B. Suryamas, F. Iskandar, K. Okuyama, Scaling law on particle-to-fiber formation during electrospinning, Polymer 50(20) (2009) 4935-4943.

[44] S. Kim, C.A. Scholes, D.E. Heath, S.E. Kentish, Gas-liquid membrane contactors for carbon dioxide separation: A review, Chem. Eng. J. 411 (2021) 128468.

[45] A. Lafuma, D. Quéré, Superhydrophobic states, Nater Mater. 2(7) (2003) 457-460.

[46] S.H. Park, J.H. Kim, S.J. Moon, E. Drioli, Y.M. Lee, Enhanced, hydrophobic, fluorine-containing, thermally rearranged (TR) nanofiber membranes for desalination via membrane distillation, J. Membr. Sci. 550 (2018) 545-553.

[47] L.D. Tijing, Y.C. Woo, W.-G. Shim, T. He, J.-S. Choi, S.-H. Kim, H.K. Shon, Superhydrophobic nanofiber membrane containing carbon nanotubes for high-performance direct contact membrane distillation, J. Membr. Sci. 502 (2016) 158-170.

[48] A. Portugal, J. Sousa, F. Magalhães, A. Mendes, Solubility of carbon dioxide in aqueous solutions of amino acid salts, Chem. Eng. Sci. 64(9) (2009) 1993-2002.

[49] E. Hosseini, G.W. Stevens, C.A. Scholes, Membrane gas-solvent contactors undergoing oscillating solvent flow for enhanced carbon dioxide capture, Sep. Purif. Technol. 227 (2019) 115653.

[50] P.D. Vaidya, P. Konduru, M. Vaidyanathan, E.Y. Kenig, Kinetics of Carbon Dioxide Removal by Aqueous Alkaline Amino Acid Salts, Ind. Eng. Chem. Res. 49(21) (2010) 11067-11072.

[51] G. Hu, K.H. Smith, Y. Wu, K.A. Mumford, S.E. Kentish, G.W. Stevens, Carbon dioxide capture by solvent absorption using amino acids: A review, Chinese Journal of Chemical Engineering 26(11) (2018) 2229-2237.

[52] J.P. Holman, Heat Transfer, 7th Edition ed., McGraw-Hill, New York, 1990.